Systems/Circuits

Anterolateral Motor Cortex Connects with a Medial Subdivision of Ventromedial Thalamus through Cell Type-Specific Circuits, Forming an Excitatory Thalamo-Cortico-Thalamic Loop via Layer 1 Apical Tuft Dendrites of Layer 5B Pyramidal Tract Type Neurons

KuangHua Guo,[1] Naoki Yamawaki,[1] Karel Svoboda,[2] and Gordon M.G. Shepherd[1]

[1]Department of Physiology, Feinberg School of Medicine, Northwestern University, Chicago, Illinois 60611, and [2]Janelia Research Campus, Howard Hughes Medical Institute, Ashburn, Virginia 20147

The anterolateral motor cortex (ALM) and ventral medial (VM) thalamus are functionally linked to support persistent activity during motor planning. We analyzed the underlying synaptic interconnections using optogenetics and electrophysiology in mice (female/male). In cortex, thalamocortical (TC) axons from VM thalamus excited VM-projecting pyramidal tract (PT) neurons in layer 5B of ALM. These axons also strongly excited layer 2/3 neurons (which strongly excite PT neurons, as previously shown) but not VM-projecting cortico-thalamic (CT) neurons in layer 6. The strongest connections in the VM → PT circuit were localized to apical tuft dendrites of PT neurons, in layer 1. These tuft inputs were selectively augmented after blocking hyperpolarization-activated cyclic nucleotide-gated (HCN) channels. In thalamus, axons from ALM PT neurons excited ALM-projecting VM neurons, located medially in VM. These axons provided weak input to neurons in mediodorsal nucleus, and little or no input either to neurons in the GABAergic reticular thalamic nucleus or to neurons in VM projecting to primary motor cortex (M1). Conversely, M1 PT axons excited M1- but not ALM-projecting VM neurons. Our findings indicate, first, a set of cell type-specific connections forming an excitatory thalamo-cortico-thalamic loop for ALM ↔ VM communication and a circuit-level substrate for supporting reverberant activity in this system. Second, a key feature of this loop is the prominent involvement of layer 1 synapses onto apical dendrites, a subcellular compartment with distinct signaling properties, including HCN-mediated gain control. Third, the segregation of the ALM ↔ VM loop from M1-related circuits of VM adds cellular-level support for the concept of parallel pathway organization in the motor system.

Key words: corticothalamic; layer 1; motor cortex; thalamocortical; ventromedial thalamus

Significance Statement

Anterolateral motor cortex (ALM), a higher-order motor area in the mouse, and ventromedial (VM) thalamus are anatomically and functionally linked, but their synaptic interconnections at the cellular level are unknown. Our results show that ALM pyramidal tract neurons monosynaptically excite ALM-projecting thalamocortical neurons in a medial subdivision of VM thalamus, and vice versa. The thalamo-cortico-thalamic loop formed by these recurrent connections constitutes a circuit-level substrate for supporting reverberant activity in this system.

Introduction

The mammalian motor cortex comprises multiple subregions, the differentiated functions of which involve interactions with an array of motor-related thalamic nuclei (Strick, 1986; Middleton and Strick, 2000; Jones, 2007; Bosch-Bouju et al., 2013). Anatomically, primary motor cortex (M1) receives particularly prominent projections from the cerebellar-recipient ventral lateral (VL) nucleus (Strick and Sterling, 1974; Jones, 1975; Kuramoto et

Received May 25, 2018; revised Aug. 3, 2018; accepted Aug. 9, 2018.

Author contributions: K.G., N.Y., K.S., and G.M.G.S. designed research; K.G. performed research; K.G., and G.M.G.S. analyzed data; K.G., K.S., and G.M.G.S. wrote the paper.

The authors declare no competing financial interests.

This research was supported by National Institutes of Health Grants T32-MH-067564 (K.G.) and R01-NS-061963 (G.M.G.S.). We thank N. Bernstein and C. Maguire for technical assistance. We also thank L. Acsády for discussions and suggestions, and J. Barrett and H. Inagaki for comments on the manuscript.

Correspondence should be addressed to Gordon M.G. Shepherd, Department of Physiology, Feinberg School of Medicine, Northwestern University, Chicago, IL 60611. E-mail: g-shepherd@northwestern.edu.

DOI:10.1523/JNEUROSCI.1333-18.2018

 0270-6474/18/388787-11$15.00/0

al., 2009). M1 also receives projections from basal ganglia-recipient nuclei, particularly the ventral anterior nucleus (Strick, 1975; Kuramoto et al., 2009). The ventral medial (VM) nucleus, which is both basal ganglia and cerebellar recipient (Groenewegen and Witter, 2004; Gao et al., 2018), sends projections to multiple motor areas, particularly premotor and other higher-order areas in frontal cortex (Herkenham, 1979; Arbuthnott et al., 1990; Kuramoto et al., 2015). In rodents, the medial subdivision of the posterior nucleus (POm), which receives ascending paralemniscal somatosensory afferents, projects to M1 (in addition to somatosensory cortex; Hooks et al., 2013). The intracortical connections of some of these projections, particularly VL → M1 and POm → M1, have begun to be elucidated in mice (Hooks et al., 2013; Yamawaki et al., 2014; Yamawaki and Shepherd, 2015), as have projections of VM → medial prefrontal cortex (mPFC; Cruikshank et al., 2012; Collins et al., 2018). However, the cellular circuits that link premotor and other higher-order motor cortical areas with VM remain to be characterized.

In the mouse, the anterolateral motor (ALM) cortex has premotor-like properties, particularly in behavioral tasks involving motor planning during a temporal delay (Guo et al., 2014; Inagaki et al., 2018). ALM neurons show persistent activity anticipating specific movements, seconds before movement onset. These studies have implicated strong bidirectional interactions between ALM and the thalamus, including the VM nucleus, as being crucial for these behavioral functions (Guo et al., 2017). The ALM-recipient subdivision of VM receives input from substantia nigra pars reticulata as well as the fastigial nucleus of the cerebellum (Gao et al., 2018). The cellular-level excitatory connections that form thalamo-cortico-thalamic (T-C-T) circuits in this system remain unknown.

The goal of this study was to characterize these connections in the putative T-C-T loop involving ALM and VM, focusing on the identification of connections onto back-projecting neurons in either area, which would form a basis for recurrent excitation in this system. We used previously developed strategies for cell type-specific circuit analysis based on combining optogenetic photostimulation with electrophysiological recordings from retrogradely labeled projection neurons in motor cortex and motor thalamus (Yamawaki and Shepherd, 2015; Yamawaki et al., 2016). Our results delineate a set of cell type-specific excitatory connections constituting the cellular and synaptic underpinnings of a bidirectional ALM ↔ VM T-C-T loop.

Materials and Methods

Animals

Animal studies followed the guidelines of the National Institutes of Health and Society for Neuroscience, and were approved by the Northwestern University Animal Care and Use Committee. The following mouse strains were used in these studies, maintained as in-house breeding colonies. For wild-type mice (WT) we used either C57BL/6 mice or Gad2-mCherry mice (Gad2-T2a-NLS-mCherry, The Jackson Laboratory; RRID:IMSR_JAX:023140). For cell type-specific expression, we used the Cre lines Rbp4-Cre (Rbp4_KL100-Cre, MMRRC; RRID:MMRRC_037128-UCD; Gerfen et al., 2013), Ntsr1-Cre (Ntsr1_GN220-Cre, MMRRC; RRID:MMRRC_030648-UCD; Gong et al., 2007), and Calb1-Cre (Calb1-IRES2-Cre-D, The Jackson Laboratory; RRID:IMSR_JAX:028532), each back-crossed with C57BL/6 mice for at least six generations. A Cre-dependent tdTomato line (Ai14, The Jackson Laboratory; RRID:IMSR_JAX:007908; Madisen et al., 2015) was used as a fluorescent reporter. Female and male mice were used in approximately equal numbers. Animals were housed with a 12 h light/dark cycle, with *ad libitum* access to water and food. Mice were 1.5–3 months old at the time of the initial surgery and were used for experiments 3–6 weeks later. Animal numbers for each type of experiment are given in the text and figures.

Labeling

Stereotaxic injections were performed as described previously (Yamawaki and Shepherd, 2015). Briefly, mice were deeply anesthetized with isoflurane and placed in a stereotaxic frame. Ophthalmic ointment was applied to protect the eyes during surgery. Thermal support was provided using a feedback-controlled heating pad (Warner). Mice were given preoperative analgesic coverage (buprenorphine 0.3 mg/kg, s.c.). Small craniotomies were opened directly over cortical and/or subcortical targets in the right hemisphere. Injection pipettes were fabricated from glass capillary micropipettes (Wiretrol II, Drummond Scientific Company) by pulling (PP-830, Narishige) to a fine tip and beveling (Micro Grinder EG-400, Narishige) to a sharp edge. Pipettes were loaded with virus or tracer solution by tip filling (i.e., application of negative pressure to the back of the pipette). Pipettes were advanced slowly to their targets, where 40–100 nl of virus was injected, and were kept in place for several minutes before retraction. Animals received postoperative analgesic coverage (meloxicam 1.5 mg/kg, s.c., once every 24 h for 2 d) and were maintained for at least 3 weeks before slice experiments. The experiment-specific details are as follows.

In experiments examining thalamic input to cortical neurons, in most cases adeno-associated virus (AAV)-channelrhodopsin-2 (ChR2)-Venus (AAV1.CAG.ChR2-Venus.WPRE.SV40, AV-1-PV2126; University of Pennsylvania Vector Core) was injected into thalamus of WT mice or Gad2-mCherry mice (which in these experiments were used simply as a source of wild-type mice, not for their labeling pattern). For VM injections, the stereotaxic coordinates were as follows: 1.3–1.7 mm posterior to bregma; 0.8–1.0 mm lateral to midline; and 4.1–4.4 mm below pia. After virus injection, additional injections were made with either latex microspheres (red Retrobeads, LumaFluor) or cholera toxin subunit B conjugated to Alexa Fluor (CTB647, Life Technologies) to retrogradely label projection neurons in ALM. Specifically, tracers were injected into VM (same coordinates as above) to label both pyramidal tract (PT) and layer 6 corticothalamic (CT) neurons, and into pons (3.5–3.7 mm posterior; 0.4–0.6 mm lateral; 5.0–5.8 mm deep) to label PT neurons.

In a subset of the thalamocortical (TC) experiments, AAV-FLEX-ChR2-tdTomato (AAV1.CAGGS.FLEX.ChR2-tdTomato.WPRE.SV40, AV-1-18917P; University of Pennsylvania Vector Core) was injected into VM of Calb1-Cre mice. These mice were used to explore the possibility of facilitating selective labeling of VM, which, characteristic of matrix-type thalamic nuclei, expresses calbindin at relatively high levels (Jones, 2001; Rubio-Garrido et al., 2007). In Calb1-Cre mice, Cre expression is relatively high in VM (transgenic characterizations #574212675, #576527875, and #576528091, Allen Brain Institute; http://connectivity.brain-map.org/transgenic). However, injections targeted to VM resulted in similar labeling patterns in thalamus using either the Cre-dependent or Cre-independent approach, and electrophysiological results were also statistically indistinguishable; the results were therefore pooled.

In experiments examining cortical input to thalamic neurons, we used Rbp4-Cre and Ntsr1-Cre mice to selectively label the PT or CT components, respectively, that together comprise the cortical projection to thalamus. Previous studies have characterized the cellular specificity of Cre expression in cortical neurons in these lines [Gong et al., 2007; Gerfen et al., 2013; Bortone et al., 2014; multiple transgenic characterizations available at http://connectivity.brain-map.org/transgenic (e.g., #167642756 for Rbp4-Cre)] and have used these lines for selectively labeling the PT and CT components of the cortical projection to thalamus (Grant et al., 2016; Jeong et al., 2016). Specifically, AAV-FLEX-ChR2-tdTomato (for details, see above) was injected into the ALM of either Ntsr1-Cre mice, to label layer 6 CT neurons, or Rbp4-Cre mice, to label layer 5 intratelencephalic and PT neurons. Injection of the same Cre-dependent virus into the cortex of WT mice resulted in no labeling ($n = 2$). The ALM and M1 were also injected with retrograde tracer to label thalamocortical neurons in VM. The ALM coordinates (Komiyama et al., 2010; Guo et al., 2014) were as follows: 2.4–2.6 mm anterior; 1.4–1.6 mm lateral; and 0.1–1.7 mm deep. The M1 coordinates were as follows: 0.1–0.3 mm posterior; 1.5–1.7 mm lateral; and 0.1–1.0 mm deep. To characterize the Cre ex-

pression of ALM PT neurons in Rbp4-Cre mice, a Cre-dependent retrograde AAV (Tervo et al., 2016), AAVretro-FLEX-tdTomato (retrograde AAV #28306; Addgene), was injected into VM.

Circuit analysis

Brain slices were prepared as described previously (Yamawaki and Shepherd, 2015). Briefly, mice that had undergone *in vivo* labeling were killed by anesthetic overdose and decapitation. Brains were rapidly removed and placed in chilled cutting solution (composition, in mM: 110 choline chloride, 11.6 sodium L-ascorbate, 3.1 pyruvic acid, 25 $NaHCO_3$, 25 D-glucose, 2.5 KCl, 7 $MgCl_2$, 0.5 $CaCl_2$, and 1.25 NaH_2PO_4, aerated with 95% O_2/5% CO_2). For experiments involving cortical recordings, brains were trimmed using blocking cuts angled to yield off-sagittal slices (0.3 mm) that optimally preserved the apical dendrites of cortical pyramidal neurons. For thalamic recordings, blocking cuts were angled to yield coronal slices (0.25 mm) containing the ventral thalamus. Slices were cut (VT1200S, Leica) in chilled cutting solution, and transferred to artificial CSF (ACSF), composed of the following (in mM): 127 NaCl, 25 $NaHCO_3$, 25 D-glucose, 2.5 KCl, 1 $MgCl_2$, 2 $CaCl_2$, and 1.25 NaH_2PO_3. Slices were incubated for 30 min at 34°C, and then kept at 22°C for at least an hour before recording.

Electrophysiology and photostimulation. Brain slices were transferred to the recording chamber of an upright microscope (BX51WI chassis, Olympus) equipped for whole-cell electrophysiology and photostimulation, as previously described (Yamawaki and Shepherd, 2015). The bath solution consisted of ACSF warmed to 34°C by an in-line feedback-controlled heater (TC 324B, Warner). For all cortical recordings, tetrodotoxin (TTX; 1 μM; Tocris Bioscience) and 4-aminopyridine (4AP; 100 μM; Sigma-Aldrich) were added to the ACSF to isolate monosynaptic (i.e., eliminate intracortical polysynaptic) inputs (Petreanu et al., 2009); these reagents were omitted for recordings in thalamus, where intrathalamic polysynaptic excitation was not a concern. For recordings in cortex, 3-(2-carboxypiperazin-4-yl)propyl-1-phosphonic acid (CCP, 5 μM; Tocris Bioscience) and ZD7288 (10 μM; Tocris Bioscience) were included to block NMDA receptors and hyperpolarization-activated cyclic nucleotide-gated (HCN) channels, respectively.

Patch pipettes were fabricated by pulling (P-97; Sutter Instrument) borosilicate glass (inner diameter, 0.86; outer diameter, 1.5 mm; with filament; Warner) to a fine tip (resistance, 2–4 MΩ). Recordings were made in voltage-clamp or current-clamp mode using pipettes filled with cesium- or potassium-based internal solution (composition, in mM: 128 cesium or potassium methanesulfonate, 10 HEPES, 10 phosphocreatine, 4 $MgCl_2$, 4 ATP, 0.4 GTP, 3 ascorbate, 1 EGTA, 1 QX-314, 0.05 Alexa Fluor hydrazide, and 4 mg/ml biocytin, pH 7.25, 290–295 mOsm).

A video camera (Retiga 2000r, Q-Imaging) was used to image slices and cells under wide-field gradient-contrast or epifluorescence optics. Labeling patterns of retrogradely labeled somata and anterogradely labeled axons were visualized using LED illumination (catalog #M470L2, #M530L2, and #M660L3, Thorlabs) and standard filter sets (catalog #U-N41017, #U-N31002, Chroma, #CY5-4040C-OMF, Semrock). Pipettes were advanced under positive pressure to establish >1 GΩ seals onto identified neurons. After membrane rupture to establish whole-cell configuration, intracellular recordings were made with an amplifier (Multiclamp 700B, Molecular Devices). Recordings with series resistance of >40 MΩ were excluded.

For wide-field photostimulation, as previously described (Yamawaki and Shepherd, 2015), a blue LED (catalog #M470L2, Thorlabs) was driven with a TTL (transistor–transistor logic) pulse to generate photostimuli with a duration of 5 ms. The LED intensity controller was set to deliver 1 mW/mm^2 at the level of the specimen. For each cell, photostimulation trials were repeated three times at an interstimulus interval of 30 s while recording in voltage-clamp mode with the command potential set to −70 mV.

For subcellular circuit mapping (sCRACM; Petreanu et al., 2009), a blue laser (473 nm, 50 mW; model MLL-FN473, CNI Laser) and scan system (model 6210 galvanometer pair, Cambridge Technology) were used for focal photostimulation and subcellular mapping, as previously described (Petreanu et al., 2009; Suter and Shepherd, 2015). Photostimuli were generated by controlling an electro-optical modulator (350–50, 302 RM, Conoptics) and mechanical shutter (LS2ZM2, VCM-D1, Uniblitz) in the beam path to produce a 1.0-ms-duration pulse of light at each stimulus location. The intensity was in the range of 0.1–2 mW/mm^2 at the level of the specimen, adjusted on a cell-by-cell basis to generate a 100–200 pA response to stimulation near the soma. Stimulation grids consisted of at least 26 rows and 10 columns, with uniform 60 μm spacing. The upper edge of the grid (row 1) was aligned to the pia, and the grid was horizontally centered over the soma. The grid parameters (total area, ~1 mm^2; ~250 sites/mm^2) and orientation were chosen to extend from pia to white matter and fully span the dendritic arbors of PT neurons. Each neuron was mapped three times using different pseudorandom sequences, with an interstimulus interval of 0.4 s. Ephus software (Suter et al., 2010) was used to control hardware settings and other parameters for coordinating photostimulation and electrophysiology data acquisition.

Analysis. To quantify LED-evoked responses, for each cell, the traces from several (generally three) trial repetitions were averaged, and the response amplitude was calculated as the mean amplitude in a post-stimulus interval of 50 ms. Data were compared by pooling across slices and animals, as in previous studies (Yamawaki and Shepherd, 2015). Pairwise comparisons were made using the absolute or normalized response amplitudes, as indicated in the text. To quantify sCRACM data, the traces from the three map trials were averaged, mean response amplitudes were determined as described above, and these values were used to construct maps representing the synaptic input at each stimulus location.

Experimental design and statistical analysis

Group comparisons were made using nonparametric tests as indicated in the text, with significance defined as $p < 0.05$. Unpaired data were compared using the rank-sum test. Paired data were compared using the sign test. For group data, median and median average deviation (m.a.d.) values were calculated as descriptive statistical measures of central tendency and dispersion, except for ratios, for which geometric means and standard factors were calculated. Statistical analyses were conducted using standard Matlab (MathWorks) functions.

Results

Excitatory input from VM thalamocortical axons to VM-projecting ALM neurons is much stronger to layer 5B PT neurons than to layer 6 CT neurons

To dissect the cell type-specific connections at the cortical end of the potential T-C-T loop, we photostimulated ChR2-expressing TC axons from VM in cortical brain slices while recording from cortical projection neurons in ALM. First, we localized ALM-projecting VM neurons ($VM^{ALM\text{-}proj}$) by injecting ALM with retrograde tracer and imaging the thalamus (Fig. 1*A*). Next, in different animals, we targeted this VM region for injection with AAV-ChR2-Venus to label VM projections, and also with a retrograde tracer to label VM-projecting cortical neurons (Fig. 1*B*). In the same animals, we also injected the pons with retrograde tracer to label PT neurons and thereby identify layer 5B (Qiu et al., 2011). This approach yielded triple-labeled cortical slices (Fig. 1*C*). Anterogradely labeled axons from TC neurons in VM were densest in layer 1 (Herkenham, 1979; Arbuthnott et al., 1990; Kuramoto et al., 2015). The slices also contained the retrogradely labeled pons-projecting neurons, demarcating layer 5B, and the retrogradely labeled thalamus-projecting neurons in both layers 5B and 6. For clarity and consistency with previous studies, we refer to the thalamus-projecting neurons in layer 5B as PT neurons (i.e., with thalamic branches), and those in layer 6 as CT neurons (Harris and Shepherd, 2015; Yamawaki and Shepherd, 2015).

With this labeling approach, we investigated excitatory connectivity in the VM → ALM pathway, initially focusing on these two types of VM-projecting neurons: layer 5B PT neurons and

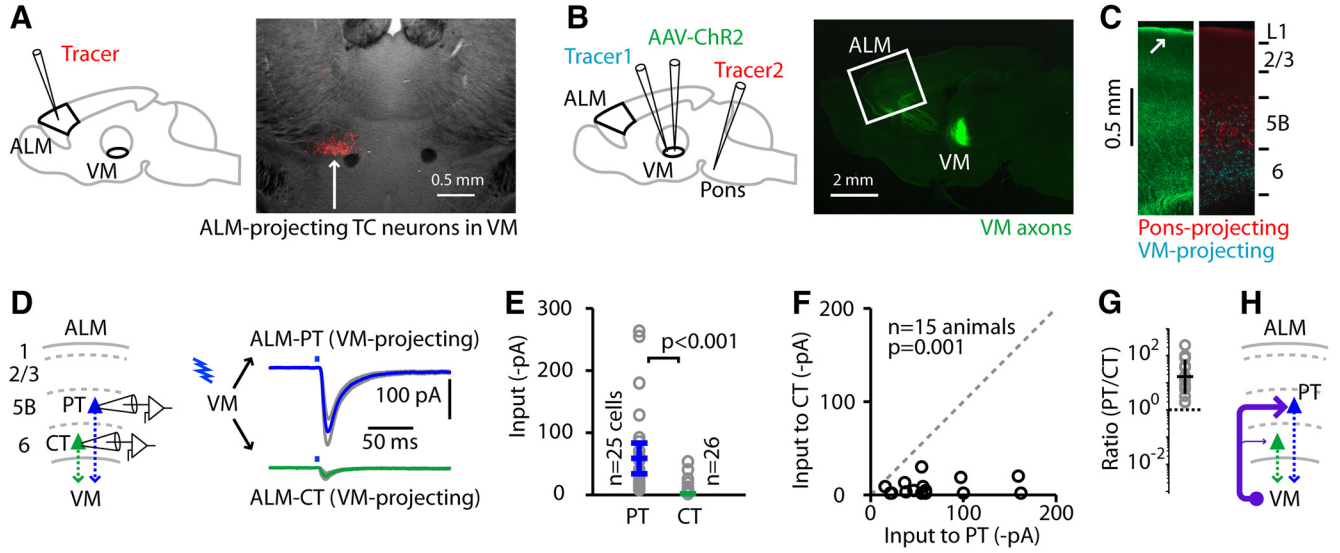

Figure 1. Excitatory input from VM TC axons to VM-projecting ALM neurons is much stronger to layer 5B PT neurons than to layer 6 CT neurons. ***A***, Fluorescence image (right) showing ALM-projecting TC neurons in VM following injection of retrograde tracer into ALM (left). ***B***, Left, Strategy for retrogradely labeling ALM PT and CT neurons from the pons and thalamus, and for anterogradely labeling thalamocortical projections from VM. Right, Fluorescence image showing projections of TC axons from VM following the injection of AAV-ChR2-Venus into VM in a wild-type animal. White box: anterior cortex, including ALM. ***C***, Cortical labeling pattern in ALM slices following the injections depicted in ***B***, with VM axons (left, green) at particularly high density in layer 1 (arrow); demarcation of layer 5B by retrograde labeling of pons-projecting PT neurons (right, red); and labeling (cyan) of both VM-projecting PT neurons (in layer 5B) and CT neurons (in layer 6). ***D***, Monosynaptic EPSCs recorded in VM-projecting PT (blue) and CT (green) neurons in ALM, evoked by a brief photostimulus (blue bars above traces) to activate ChR2-expressing VM axons, in the presence of TTX and 4AP (see Materials and Methods). Traces represent group-averaged responses (±SEM; gray lines). ***E***, Cell-based group comparison. Input to PT and CT neurons (circles). Error bars represent the median input across cells (±m.a.d.). Results for WT and Calb1-Cre mice were similar and therefore pooled for analysis. The *p* value for the rank-sum test comparing the two groups is shown, along with the numbers of cells per group. ***F***, Animal-based group comparison. Pairwise comparison of input to the same groups of PT and CT neurons, averaged by animal (each datum represents one animal). The *p* value for the sign test comparing the two groups is shown, along with the number of animals. ***G***, Animal-based ratios. The ratio of input to PT divided by input to CT is shown for each animal (circles), along with the geometric mean and the geometric standard factor (bars). ***H***, Schematic depiction of the cellular connectivity pattern.

layer 6 CT neurons (Fig. 1*D*). Photostimulation of the VM axons (with TTX and 4AP in the bath solution; see Materials and Methods), generated fast, large, monosynaptic excitatory currents in VM-projecting PT neurons that were much stronger than the generally weak or undetectable responses recorded in VM-projecting CT neurons (Fig. 1*D–G*). Findings were similar with wild-type mice and Calb1-Cre mice (Materials and Methods), and the data were therefore pooled for analysis (Fig. 1*D–G*). Findings were similar for group comparisons based on individual neurons (Fig. 1*E*) or animals (Fig. 1*F*,*G*).

Specifically, for WT mice ($n = 8$), injected in VM with AAV-ChR2-Venus, the VM → PT responses were approximately −50 pA [median across $n = 14$ cells, −56.7 ± 31.7 pA (median ± m.a.d.); median for $n = 8$ mice, −54.6 ± 32.7 pA] while the VM → CT responses were less than −5 pA (median across $n = 13$ cells, −1.3 ± 1.1 pA; median for $n = 8$ mice, −1.0 ± 0.5 pA), a 10-fold difference (unpaired cell-based comparison, $p = 0.0002$, rank-sum test; pairwise animal-based comparison, $p = 0.008$, sign test; VM → PT/VM → CT ratio per animal, 19.9 ± 5.9, geometric mean ± geometric standard factor). For Calb1-Cre mice ($n = 7$) injected in VM with AAV-FLEX-ChR2-tdTomato, the VM → PT responses were approximately −50 pA (median across $n = 11$ cells, −58.2 ± 12.2 pA; median for $n = 7$ mice, −55.9 ± 18.3 pA), whereas the VM → CT responses were less than −5 pA (median across $n = 13$ cells, −3.7 ± 3.1 pA; median for $n = 7$ mice, −3.8 ± 2.8 pA), a statistically significant difference (unpaired cell-based comparison, $p = 0.0001$, rank-sum test; pairwise animal-based comparison, $p = 0.016$, sign test; VM → PT/ VM → CT ratio per animal, 12.9 ± 2.9, geometric mean ± geometric standard factor). For the pooled data ($n = 15$ mice total, WT and Calb1-Cre), the VM → PT responses were approximately −50 pA (median across $n = 25$ cells, −58.2 ± 24.1 pA; median for $n = 15$ mice, −54.7 ± 18.2 pA), while the VM → CT responses were less than −5 pA (median across $n = 26$ cells, −1.7 ± 1.6 pA; median for $n = 15$ mice, −3.7 ± 3.1 pA), a statistically significant difference (unpaired cell-based comparison, $p = 4 \times 10^{-8}$, rank-sum test; pairwise animal-based comparison, $p = 0.0001$, sign test; VM → PT/VM → CT ratio per animal, 16.3 ± 4.3, geometric mean ± geometric standard factor).

These results show that VM projections to ALM excite VM-projecting PT neurons, with little or no input to back-projecting CT neurons (Fig. 1*H*). An important implication of this result (addressed in experiments presented in a later section) is that if the potential ALM ↔ VM T-C-T loop is tightly "closed" by monosynaptic connections, such connections must involve the PT neurons, rather than the CT neurons, given the prevalence of monosynaptic VM → PT and the paucity of VM → CT connections.

VM axons also strongly excite layer 2/3 neurons in ALM

We also considered the possibility of strong VM inputs to layer 2/3 pyramidal neurons, both because their apical dendrites arborize in layer 1, making such a connection likely by virtue of axodendritic overlap, and because layer 2/3 → PT connections are among the strongest excitatory intracortical connections in anterior motor cortex (Qiu et al., 2011), making such a connection significant by virtue of delineating a parallel disynaptic pathway (i.e., VM → 2/3 → PT). To test this, we used the same approach as above, recording from layer 2/3 pyramidal neurons and PT neurons in ALM slices while photostimulating VM axons (Fig. 2*A*). Analysis of the photo-evoked EPSCs showed about twice as much input to layer 2/3 neurons as to PT neurons (Fig. 2*B–D*). Specifically, for WT and Calb1-Cre mice ($n = 10$ mice

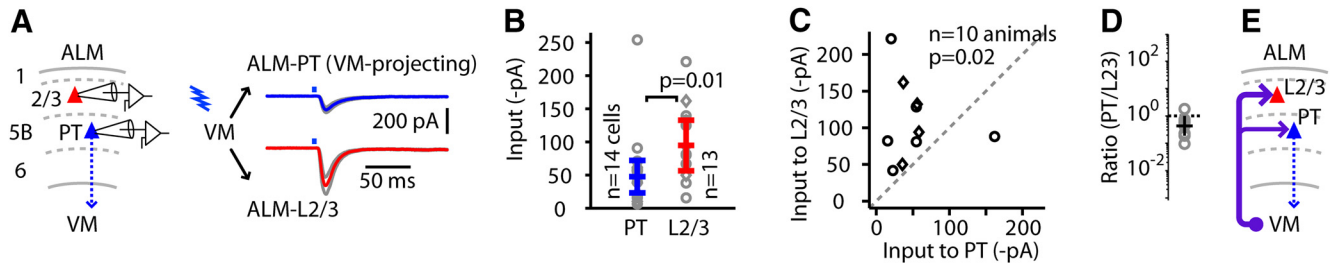

Figure 2. VM axons also strongly excite layer 2/3 neurons in ALM. ***A***, Similar to Figure 1*D*, but comparing VM input to VM-projecting PT (blue) vs layer 2/3 neurons (red). Results for WT mice (circles) and Calb1-Cre mice (diamonds) were similar and pooled for analysis. ***B***, Cell-based group comparison. ***C***, Animal-based group comparison. ***D***, Animal-based ratios. ***E***, Schematic depiction of the cellular connectivity pattern.

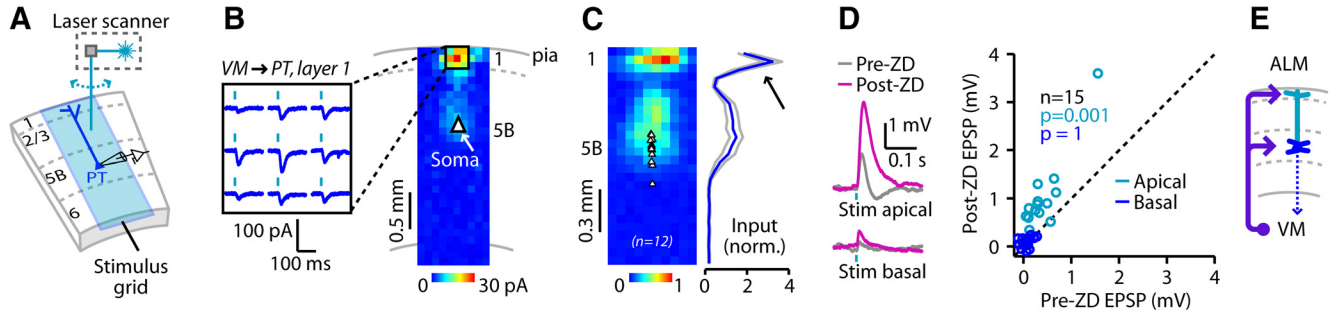

Figure 3. Localization of VM excitatory synapses to apical tuft dendrites of PT neurons. ***A***, Recording arrangement for sCRACM mapping of the locations of presynaptic VM terminals across the dendritic arbors of VM-projecting PT neurons. The top edge of the stimulus grid was aligned to the pia, and a laser beam controlled by mirror galvanometers was used to sequentially stimulate each location in a stimulus grid consisting of ≥260 sites. ***B***, Example map showing strong monosynaptic excitatory input to layer 1 dendrites of a VM-projecting ALM PT neuron. ***C***, Average map for $n = 12$ VM-projecting PT neurons. Several rows at the bottom are not shown as there was no input. Plot to the right shows the average (±SEM; gray lines) across maps of the summed input per map row. Note strong input to layer 1 dendrites (arrow). ***D***, Left, Voltage responses to focal photostimulation of VM inputs to apical and basal dendrites of a VM-projecting PT neuron, before (gray) and after (magenta) bath application of ZD7288 (10 μM) to block H-current. Right, Comparison of response amplitudes (calculated as the average voltage from 0 to 250 ms poststimulus) before and after ZD7288 (ZD), evoked by the activation of VM inputs to apical (cyan) and basal (blue) dendrites of VM-projecting PT neurons. The *p* values are for the sign test comparing response amplitudes before and after ZD application for each group, along with the number of neurons. ***E***, Schematic depiction of the subcellular connectivity pattern. norm., normalized; Stim, Stimulation.

total, pooled from 6 WT and 4 Calb1-Cre mice as the results were similar), the VM → PT responses were approximately −50 pA (median across $n = 14$ cells, −47.1 ± 25.1 pA; median for $n = 10$ mice, −46.0 ± 11.2 pA) while the VM → L2/3 responses were approximately −100 pA (median across $n = 13$ cells, −93.7 ± 38.3 pA; median for $n = 10$ mice, −91.0 ± 39.0 pA), a statistically significant difference (unpaired cell-based comparison, $p = 0.014$, rank-sum test; pairwise animal-based comparison, $p = 0.021$, sign test; VM → PT/VM → L2/3 ratio per animal, 0.43 ± 2.3, geometric mean ± geometric standard factor). Thus, layer 2/3 pyramidal neurons also receive strong VM excitation (Fig. 2*E*).

Localization of VM excitatory synapses to apical tuft dendrites of PT neurons

The high density of VM TC axons in layer 1 (Fig. 1*C*; Herkenham, 1979; Arbuthnott et al., 1990; Kuramoto et al., 2015) presents the likelihood of axodendritic overlap with the prominent apical tuft dendrites of PT neurons, which suggests that VM input to PT neurons enters via excitatory synapses on apical dendrites in layer 1. However, VM → PT EPSCs could instead or additionally reflect strong perisomatic synapses. To resolve this, we mapped the subcellular locations of inputs on postsynaptic dendrites using sCRACM (Petreanu et al., 2009; Fig. 3*A*,*B*; see Materials and Methods). These maps revealed localized hotspots of strong excitatory input to layer 1 apical tufts of PT neurons, as well as a broad region of weaker perisomatic input (Fig. 3*B*,*C*).

One implication of these synaptic mapping results is the likelihood that the tuft-targeting VM inputs are shaped by the active properties, particularly H-current (carried by HCN channels), of PT apical dendrites (Lörincz et al., 2002; Sheets et al., 2011; Larkum, 2013; Labarrera et al., 2018). To explore this, we recorded from VM-projecting ALM PT neurons (in current-clamp mode, at the resting potential) and used laser-scanning photostimulation to focally activate VM axons at one site over the apical tuft dendrites and another site over the basal dendrites close to the soma (Fig. 3*D*). Postsynaptic responses to apical stimulation were markedly enhanced after the application of ZD7288 (10 μM), a selective blocker of HCN channels, while inputs to the basal dendrites were smaller and not significantly enhanced after ZD7288 application (Fig. 3*D*).

The results of these sCRACM mapping and pharmacology experiments show that VM-projecting PT neurons in ALM receive direct, monosynaptic excitation from VM that preferentially targets apical tuft dendrites in layer 1 (Fig. 3*E*). They also demonstrate that VM → PT signaling via these distal apical inputs is modulated by H-current, suggesting a candidate mechanism for neuromodulatory regulation of VM → ALM communication.

ALM PT axons excite ALM-projecting VM TC neurons, but not M1-projecting VM TC neurons

Next, we turned our attention to the thalamus, focusing on assessing whether the axons of ALM PT neurons close the potential T-C-T loop by exciting ALM-projecting VM neurons. We used mice from the layer 5-specific Rbp4-Cre line (Materials and Methods), which enabled us to selectively photostimulate ChR2-expressing cortical axons from PT neurons (but not CT neurons) in thalamic slices. Cortical injections of AAV-FLEX-ChR2-

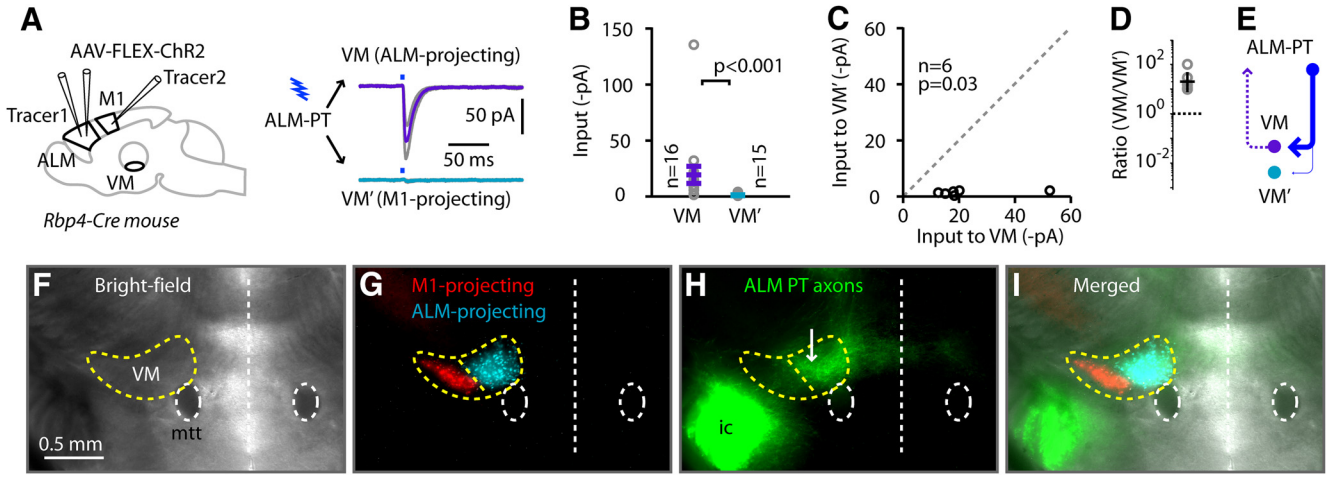

Figure 4. ALM PT axons excite ALM-projecting VM TC neurons, but not M1-projecting VM TC neurons. ***A***, Left, Schematic summary of injection strategy. Right, Average responses (±SEM; gray lines) recorded in ALM-projecting and M1-projecting VM neurons. ***B***, Cell-based group comparison. ***C***, Animal-based group comparison. ***D***, Animal-based ratios. ***E***, Schematic depiction of the cellular connectivity pattern. VM′, M1-projecting VM neurons. ***F***, Bright-field view of thalamic slice, showing VM located dorsolateral to the mammillothalamic tract (mtt). ***G***, Merged fluorescent image showing thalamic distributions of ALM-projecting (cyan) and M1-projecting (red) neurons in medial and lateral, respectively, parts of VM. ***H***, Fluorescence image of ALM PT axons (green) following the injection of AAV-FLEX-ChR2-tdTomato into ALM of an Rbp4 animal. ic, Internal capsule. ***I***, Merged image of all three channels.

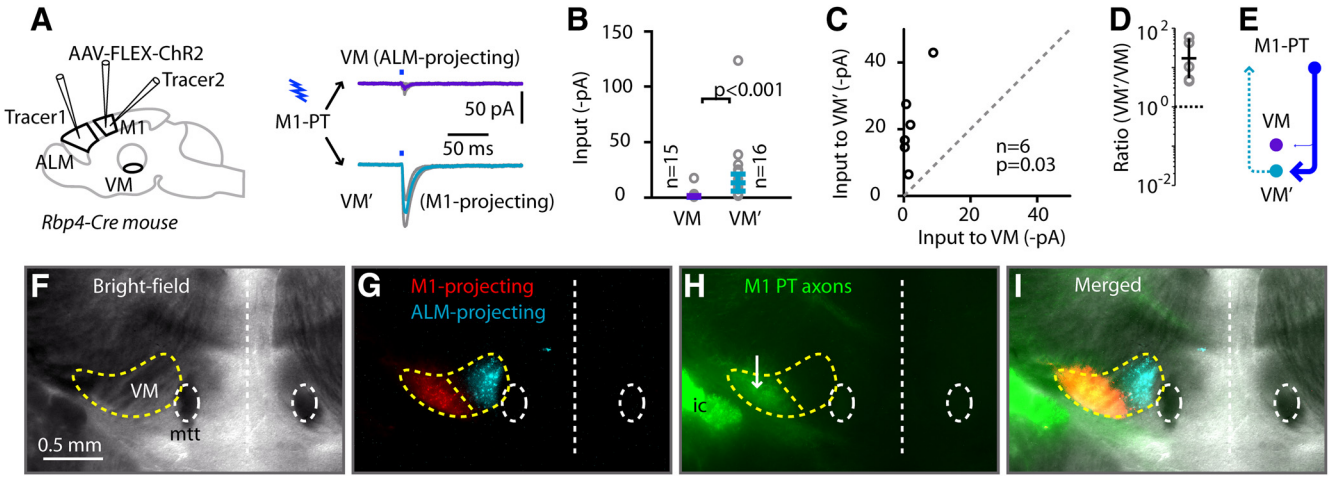

Figure 5. M1 PT axons excite M1-projecting VM TC neurons, but not ALM-projecting VM TC neurons. ***A***, Left, Schematic summary of injection strategy. Right, Average responses (±SEM; gray lines) recorded in ALM-projecting and M1-projecting VM neurons. ***B***, Cell-based group comparison. ***C***, Animal-based group comparison. ***D***, Animal-based ratios. ***E***, Schematic depiction of the cellular connectivity pattern. ***F***, Bright-field view of thalamic slice, showing VM located dorsolateral to the mammillothalamic tract (mtt). ***G***, Merged fluorescent image showing thalamic distributions of ALM-projecting (cyan) and M1-projecting (red) neurons in medial and lateral, respectively, parts of VM. ***H***, Fluorescence image of ALM PT axons (green) following injection of AAV-FLEX-ChR2-tdTomato into M1 of an Rbp4 animal. ic, Internal capsule. ***I***, Merged image of all three channels.

tdTomato and retrograde tracers into the ALM cortex of these mice yielded thalamic slices containing anterogradely labeled ChR2-expressing PT axons and retrogradely labeled ALM-projecting VM TC neurons. In addition, because VM axons can have large cortical arbors sometimes spanning multiple motor areas (Kuramoto et al., 2015) and may extend not only to ALM but also M1, we injected another retrograde tracer into M1, allowing us to compare inputs from ALM PT axons to ALM- versus M1-projecting VM TC neurons (Fig. 4*A*). Relatively strong EPSCs were detected in ALM-projecting VM TC neurons, whereas little or no input was detected in the M1-projecting VM TC neurons (Fig. 4*B–E*).

Specifically, for these experiments ($n = 6$ Rbp4-Cre mice), the responses of ALM-projecting VM neurons to ALM PT input (ALM-PT → $VM^{ALM\text{-}proj}$ responses) were approximately −20 pA (median across $n = 16$ cells, −19.1 ± 7.7 pA; median for $n = 6$ mice, −18.3 ± 2.5 pA), while the ALM-PT → M1-projecting VM neuron ($VM^{M1\text{-}proj}$) responses were nearly 0 pA (median across $n = 15$ cells, −0.7 ± 0.6 pA; median for $n = 6$ mice, −1.5 ± 0.4 pA), a statistically significant difference (unpaired cell-based comparison, $p = 0.00001$, rank-sum test; pairwise animal-based comparison, $p = 0.03$, sign test; ALM-PT → $VM^{ALM\text{-}proj}$/ALM-PT → $VM^{M1\text{-}proj}$ ratio per animal, 18.7 ± 2.5, geometric mean ± geometric standard factor).

These results show that excitatory PT → VM connections are formed onto back-projecting neurons, thus closing a T-C-T loop at the thalamic end, and that this ALM ↔ VM circuit does not engage other VM neurons that project to M1 (Fig. 4*E*). Consistent with the electrophysiological findings, the ALM-projecting TC neurons were anatomically localized to a medial part of VM, where ALM PT axons also ramified, whereas M1-projecting TC neurons were found in a more lateral part of VM (Fig. 4*F–I*). An implication of these findings is that the T-C-T loop is "closed" not only in the sense of recurrent excitatory connectivity between

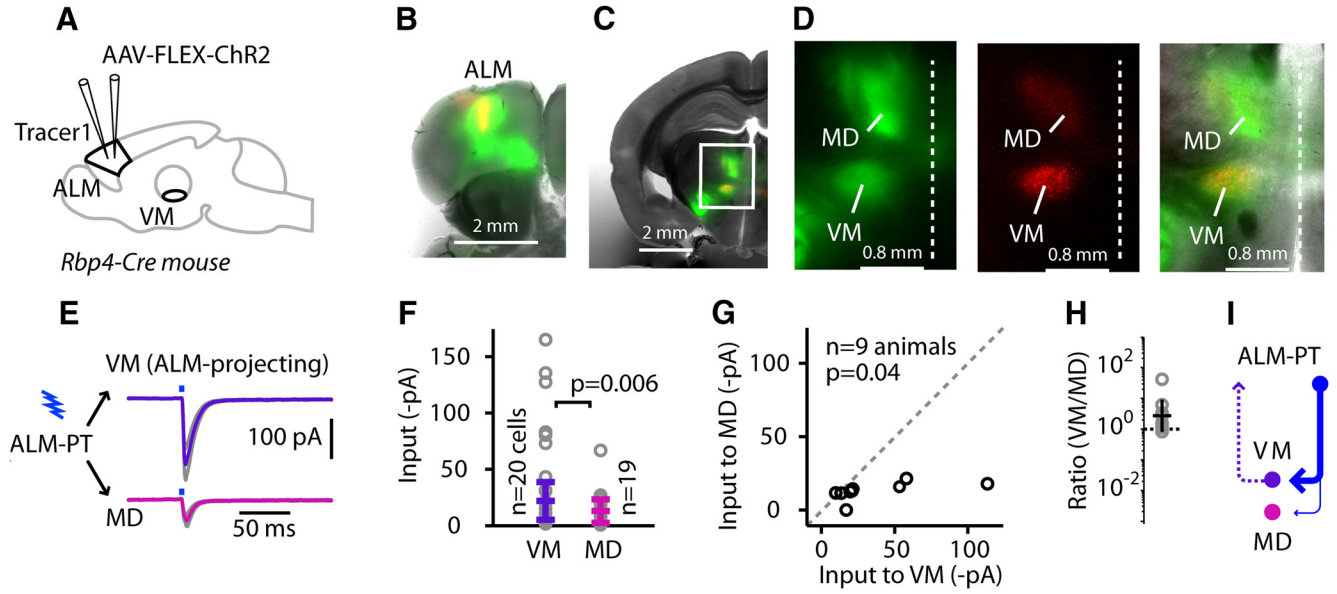

Figure 6. Excitatory input from ALM PT axons is stronger to VM than to MD. ***A***, Left, Schematic summary of injection strategy. ***B***, Merged bright-field and fluorescence image showing site of ALM injection with AAV-FLEX-ChR2-tdTomato (displayed as green) and tracer (red). ***C***, Merged image showing thalamic labeling. ***D***, Higher-magnification views of thalamus, showing labeling of ALM PT axons (left, green) and ALM-projecting (proj.) TC neurons (middle, red) separately, and in a merged image (right). ***E***, Average responses (±SEM; gray lines) recorded in ALM-projecting VM neurons and MD neurons. ***F***, Cell-based group comparison. ***G***, Animal-based group comparison. ***H***, Animal-based ratios. ***I***, Schematic depiction of the cellular connectivity pattern.

ALM and VM, but also in the sense of not engaging M1-associated T-C-T circuits.

M1 PT axons excite M1-projecting VM TC neurons, but not ALM-projecting VM TC neurons

To further explore these implications, we asked whether the converse connectivity pattern also holds; that is, do M1 PT axons preferentially excite M1-projecting rather than ALM-projecting VM TC neurons. We therefore repeated the experiment above, but injected the AAV-FLEX-ChR2-tdTomato into M1. Recordings in the thalamus from the two types of retrogradely labeled VM TC neurons showed the complementary pattern of excitatory input, with photo-evoked EPSCs detected in M1-projecting VM TC neurons but little or no input to ALM-projecting neurons (Fig. 5*A–E*). Specifically, for these experiments ($n = 6$ Rbp4-Cre mice), the M1-PT → $VM^{M1\text{-}proj}$ responses were approximately −13 pA (median across $n = 16$ cells, −13.3 ± 7.6 pA; median for $n = 6$ mice, −18.9 ± 6.5 pA), while the M1-PT → $VM^{ALM\text{-}proj}$ responses were nearly 0 pA (median across $n = 15$ cells, −0.8 ± 0.6 pA; median for $n = 6$ mice, −1.0 ± 0.7 pA), a statistically significant difference (unpaired cell-based comparison, $p = 0.00004$, rank-sum test; pairwise animal-based comparison, $p = 0.03$, sign test; M1-PT → $VM^{M1\text{-}proj}$/M1-PT → $VM^{ALM\text{-}proj}$ ratio per animal, 17.1 ± 3.2, geometric mean ± geometric standard factor). Consistent with the electrophysiological results, anatomically the M1 PT axons were found to ramify in the laterally located M1-projecting subregion of VM, rather than in the ALM-projecting subregion (Fig. 5*F–I*). These findings provide further evidence that the T-C-T loops in the motor areas are relatively segregated.

Excitatory input from ALM PT axons is stronger to VM than to mediodorsal

In addition to the dense axonal projection from ALM PT neurons to VM, axons were also observed in the mediodorsal (MD) nucleus (Fig. 6*A–D*), raising the question of the relative innervation of MD TC neurons versus ALM-projecting VM TC neurons. To resolve this, we injected the ALM of Rbp4 mice with AAV-FLEX-ChR2-tdTomato and retrograde tracer, and recorded in thalamus from MD TC neurons and ALM-projecting VM TC neurons. Although EPSCs were sometimes detected in MD TC neurons, overall these neurons received significantly weaker input compared with ALM-projecting VM TC neurons (Fig. 6*E–H*). Specifically, for these experiments ($n = 9$ Rbp4-Cre mice), the PT → VM responses were approximately −20 pA (median across $n = 20$ cells, −21.4 ± 16.8 pA; median for $n = 9$ mice, −20.1 ± 7.4 pA), while the PT → MD responses were approximately −13 pA (median across $n = 19$ cells, −12.5 ± 10.3 pA; median for $n = 9$ mice, −13.1 ± 1.6 pA), a statistically significant difference (unpaired cell-based comparison, $p = 0.006$, rank-sum test; pairwise animal-based comparison, $p = 0.039$, sign test; PT → VM/PT → MD ratio per animal, 2.7 ± 3.3, geometric mean ± geometric standard factor). Thus, these results indicate that ALM-projecting VM TC neurons, rather than MD TC neurons, are the primary thalamic targets of ALM PT axons (Fig. 6*I*).

ALM CT axons excite both reticular neurons and ALM-projecting VM neurons, while ALM PT axons excite primarily the latter

The preceding experiments focused on the input–output connections of PT neurons with thalamus, because they, rather than CT neurons, were found to form recurrent connections with VM neurons. However, CT neurons are also integral, albeit enigmatic, components of T-C-T circuits, and we therefore performed a limited set of experiments to characterize CT connectivity to thalamic neurons. To assay these connections, we used the CT-specific Ntsr1-Cre line to express ChR2 (using AAV-FLEX-ChR2-tdTomato) in ALM CT axons. Neurons in the reticular nucleus of the thalamus (RTN) and ALM-projecting VM TC neurons both received excitatory input from ALM CT axons (Fig. 7*A–F*). Specifically, for these experiments ($n = 7$ Ntsr1-Cre mice), the CT → VM responses (median across $n = 14$ cells, −14.3 ± 8.6 pA; median for $n = 7$ mice, −10.8 ± 6.7 pA) and the CT → RTN responses (median across $n = 13$ cells, −4.2 ± 3.7 pA; median for $n = 7$ mice, −6.4 ±

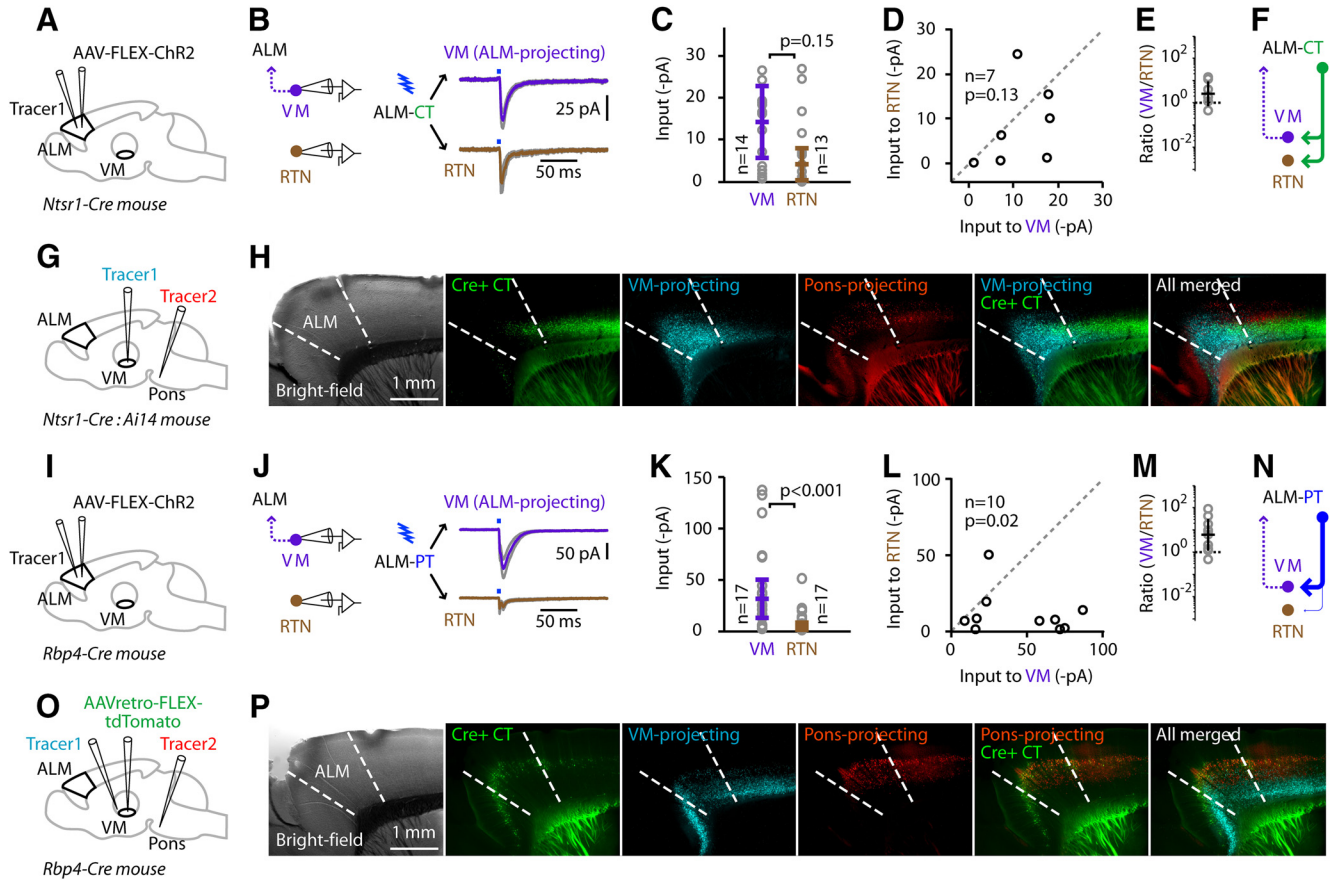

Figure 7. ALM CT axons excite both RTN and ALM-projecting VM neurons, while ALM PT axons excite primarily the latter. ***A***, Schematic of injection strategy. ***B***, Average responses (±SEM; gray lines) recorded in RTN and ALM-projecting VM neurons. ***C***, Cell-based group comparison of ALM CT input to VM-projecting VM neurons versus RTN neurons. ***D***, Animal-based group comparison. ***E***, Animal-based ratios. ***F***, Schematic depiction of the cellular connectivity patterns. ***G***, Schematic of injection strategy in Ntsr1-Cre line crossed with Ai14 reporter line. ***H***, From left to right: bright-field image, Cre^+ CT neurons labeled by tdTomato, retrogradely labeled PT and CT neurons that project to VM, retrogradely labeled PT neurons that project to pons, combined image of Cre^+ CT neurons labeled by tdTomato with retrogradely labeled PT and CT neurons that project to VM, and combined image of Cre^+ CT neurons labeled by tdTomato with retrogradely labeled PT and CT neurons that project to VM with retrogradely labeled PT neurons that project to pons. ***I***, Schematic of injection strategy. ***J***, Average responses (±SEM; gray lines) recorded in RTN and ALM-projecting VM neurons. ***K***, Cell-based group comparison of ALM PT input to VM-projecting VM neurons versus RTN neurons. ***L***, Animal-based group comparison. ***M***, Animal-based ratios. ***N***, Schematic depiction of the cellular connectivity patterns. ***O***, Schematic of injection strategy in Rbp4-Cre animal. ***P***, From right to left: bright-field image, Cre^+ PT neurons labeled by AAVretro-FLEX-tdTomato, retrogradely labeled PT and CT neurons that project to VM, retrogradely labeled PT neurons that project to pons, combined image of Cre^+ PT neurons labeled by AAVretro-FLEX-tdTomato with retrogradely labeled PT and CT neurons that project to VM, and combined image of Cre^+ PT neurons labeled by AAVretro-FLEX-tdTomato with retrogradely labeled PT and CT neurons that project to VM with retrogradely labeled PT neurons that project to pons.

5.8 pA) were not significantly different (unpaired cell-based comparison, $p = 0.15$, rank-sum test; pairwise animal-based comparison: $p = 0.13$, sign test; CT → VM/CT → RTN ratio per animal, 2.5 ± 3.6, geometric mean ± geometric standard factor). The absolute amplitudes of these ALM CT → RTN connections were notably small compared with those we previously measured for M1 CT → RTN connections (Yamawaki and Shepherd, 2015), likely reflecting the drop-off in Cre expression at the frontal pole in Ntsr1-Cre mice (Fig. 7*G*,*H*).

In contrast to ALM CT neurons, ALM PT axons provided little or no input to the RTN neurons (Fig. 7*I*–*N*). Specifically, for these experiments ($n = 10$ Rbp4-Cre mice), the PT → VM responses were approximately −35 pA (median across $n = 17$ cells, −30.7 ± 18.3 pA; median for $n = 10$ mice, −41.3 ± 26.1 pA), while the PT → RTN responses were approximately −5 pA (median across $n = 17$ cells, −3.7 ± 3.4 pA; median for $n = 10$ mice, −7.0 ± 5.6 pA), a statistically significant difference (unpaired cell-based comparison, $p = 0.001$, rank-sum test; pairwise animal-based comparison, $p = 0.021$, sign test; PT → VM/PT → RTN ratio per animal, 6.0 ± 5.2, geometric mean ± geometric standard factor). The Rbp4-Cre line had robust labeling of PT neurons in ALM (Fig. 7*O*,*P*). These experiments show that the PT neuron → VM → ALM loop is dominated by excitation, with little feedforward inhibition in the thalamus.

Discussion

Application of optogenetic-electrophysiological tools for cell type-specific analysis of excitatory connections between ALM and VM neurons yielded multiple salient details about circuit architecture in this system (Fig. 8). At the cortical end, TC → PT connections formed part of a recurrent excitatory loop, involving apical tuft dendrites of PT neurons and layer 2/3 pyramidal neurons, but not CT neurons. At the thalamic end, PT → TC connections closed the TC ↔ PT loop between ALM and VM, with weaker engagement of TC neurons in MD. The ALM ↔ VM loop involved VM TC neurons in a medial part of VM, with minimal cross talk between VM TC neurons in a more lateral, M1-associated part of VM. Collectively, these observations provide the outline of a wiring diagram describing how cortical and thalamic neurons in ALM and VM interconnect to form an excitatory T-C-T loop (Fig. 8).

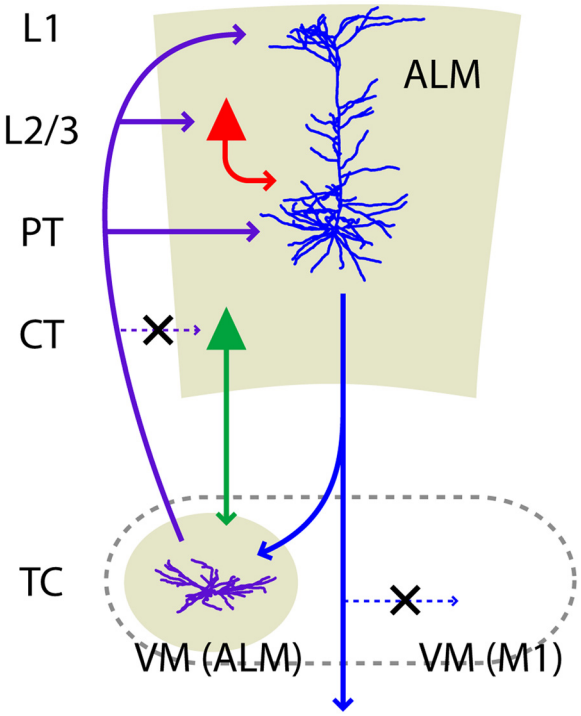

Figure 8. Schematic summary. Key connections (arrows) as well as notably weak or absent connections (marked by "X") identified in T-C-T loops of ALM and VM are depicted as a wiring diagram.

The technical approach used here has many advantages but also limitations for cell type-specific circuit analysis. For example, the combination of ChR2-based wide-field photostimulation and whole-cell recording from tracer-labeled neurons affords high selectivity for stimulating presynaptic axons of interest, high efficiency and sensitivity for detecting connections, and high specificity for sampling postsynaptic neurons of interest, thereby enabling long-range input–output connections to be determined (Luo et al., 2008; Miesenböck, 2009; Schoenenberger et al., 2011; Yamawaki et al., 2016). However, the activation of ChR2 directly at presynaptic terminals by wide-field illumination may alter synaptic release properties, potentially limiting its utility for characterizing dynamic aspects of synaptic transmission (Schoenenberger et al., 2011; Jackman et al., 2014). Laser-based focal stimulation of axons at a distance away from the recorded cell can overcome this limitation (Jackman et al., 2014) but was not attempted in this study, which focused on connectivity rather than dynamics. Moreover, our focus on excitatory connections leaves unexplored the inhibitory circuit mechanisms in this T-C-T loop. In motor cortex, different types of inhibitory interneurons are integrated into local circuits with cell-type and layer specificity (Apicella et al., 2012), and are likely to be involved in shaping responses to thalamic input similar to their roles in VM projections to mPFC (Cruikshank et al., 2012; Delevich et al., 2015; Collins et al., 2018). In motor thalamus, inhibitory inputs from both the RTN and the basal ganglia converge on VM (Jones, 2007; Kase et al., 2015). Our elucidation of excitatory connections provides a starting point for further analysis of the cellular components and biophysical properties of this T-C-T circuit.

ALM-projecting VM neurons receive cortical input from ALM PT neurons and, indeed, appear to be the main target of ALM PT inputs to thalamus, thereby closing the thalamic end of the potential loop. Together, these results demonstrate a set of cell type-specific connections forming a T-C-T loop, in which thalamic branches of PT neurons in ALM mediate recurrent connections with thalamocortical neurons in VM. This recurrent circuit architecture may relate to the physiological functions of the ALM ↔ VM circuit, by supporting persistent activity associated with motor preparation (Li et al., 2016), representing a form of short-term memory.

The axonal projections of PT neurons are diverse and complex, even among PT neurons within the same cortical area (Kita and Kita, 2012; Shepherd, 2014; Rojas-Piloni et al., 2017). Recent results indicate that VM-projecting PT neurons in ALM generate particularly early and sustained preparatory activity in a delayed-response task, contrasting with the late-preparatory and motor-command activity observed in ALM PT neurons that projects instead to medulla (Economo et al., 2018). Further studies will be needed to determine whether these two and potentially additional subtypes of ALM PT neurons also have distinct T-C-T circuit connections.

The architecture shown here for ALM has both shared and distinct features compared with T-C-T circuits of mouse M1. In both M1 and ALM, PT but not CT neurons receive direct, monosynaptic excitation from thalamus (Hooks et al., 2013; Yamawaki and Shepherd, 2015). However, the targeting of thalamic input to apical tuft dendrites is particularly strong for VM → PT connections in ALM (this study), but is relatively moderate for VL → PT connections in forelimb-related M1 (Suter and Shepherd, 2015) and relatively weak for VL → PT connections in vibrissal M1 (Hooks et al., 2013). These differences are partially explained by the anatomical differences of the TC projections: VM projections, characteristic of matrix-type TC projections, ramify densely in layer 1 (Herkenham, 1979; Arbuthnott et al., 1990; Kuramoto et al., 2015), whereas VL projections, which accord more with core-type TC projections, ramify mainly in layers 4 and 5B (Jones, 1998; Clascá et al., 2012; Yamawaki et al., 2014). Perhaps the most prominent difference between the T-C-T circuits of ALM-VM and M1-VL is that the former form a recurrent excitatory loop but the latter do not. Specifically, the finding that ALM PT neurons connect to ALM-projecting VM TC neurons (and vice versa) implies a bidirectional ALM ↔ VM circuit architecture, and contrasts with the markedly weak connections from both PT and CT neurons in M1 to M1-projecting TC neurons in VL (Yamawaki and Shepherd, 2015), which, together with robust VL → PT connections in M1 (Hooks et al., 2013; Suter and Shepherd, 2015; Yamawaki and Shepherd, 2015), implies a predominantly feedforward VL → M1 circuit architecture. These differences in functional anatomy between ALM and M1, situated at the rostral-most and caudal-most regions of the cortical motor system, presumably conform to, and likely mediate, the specialized behavioral functions associated with the two areas. In particular, ALM supports preparatory activity associated with motor planning (discussed above), while an important aspect of M1 function is to integrate cerebellar input into ongoing corticospinal activity associated with motor execution.

Recurrent connections, including direct PT ↔ TC coupling, have also recently been described linking both VM and MD with mPFC (Collins et al., 2018), another frontal area where reverberant activity is implicated in short-term mnemonic functions. In general, numerous findings underscore the many anatomical and functional commonalities across these higher-order T-C-T circuits (Jones, 2007; Cruikshank et al., 2012; Bosch-Bouju et al., 2013; Delevich et al., 2015; Alcaraz et al., 2016, 2018; Acsády, 2017; Collins et al., 2018).

Computational models have emphasized the importance of recurrent excitation to maintain persistent activity underlying short-term memory and motor planning in frontal circuits (Wang, 1999, 2001). It is usually assumed that this recurrent excitation is caused by recurrence in cortical circuits (Goldman-Rakic, 1995). However, cortical circuits are dominated by rapid and strong feedforward and feedback inhibition, which creates challenges for the maintenance of persistent activity. For these reasons biophysical models of persistent activity overcome these challenges by invoking long-duration excitatory currents. Closed T-C-T circuits producing re-entrant feedback excitation may be a key specialization whereby frontal cortical circuits maintain memory-related persistent activity over seconds. In particular, PT neurons evoke little inhibition in the thalamus and the thalamic feedback to ALM is "excitation only," overcoming the above-mentioned obstacles to the maintenance of persistent activity. This circuit may incorporate additional mechanisms, such as locally recurrent intracortical excitation, NMDA receptors, and synaptic facilitation to promote positive feedback (Wang, 1999; Wang et al., 2006; Mongillo et al., 2008; Kawaguchi, 2017). The localization of VM → PT synapses to apical tuft dendrites suggests that excitation might evoke slow dendritic spikes (Xu et al., 2012; Major et al., 2013) and involve regulation via H-current neuromodulation (Labarrera et al., 2018), which has previously been shown to regulate signaling in motor cortex circuits in a highly PT-specific manner (Sheets et al., 2011). Indeed, pharmacological blockade of HCN channels caused a marked increase in the amplitude of EPSPs generated by activating VM inputs to apical tuft dendrites of PT neurons in layer 1, indicating a candidate neuromodulatory mechanism likely to be involved in regulating activity in this T-C-T loop as well. By identifying key connections in this circuit, our results can facilitate targeted investigation of the mechanisms regulating *in vivo* activity in this system. Additionally, because aberrant activity in motor-related T-C-T loops—thalamocortical dysrhythmia—has been implicated in movement disorders (Llinás et al., 2005), our results can guide studies of pathophysiological mechanisms in disease models.

The finding that ALM PT input is specific to $VM^{ALM\text{-}proj}$ rather than $VM^{M1\text{-}proj}$ neurons was unexpected, since the wide spread of VM axons across motor cortex observed in single-axon reconstructions suggests high divergence and convergence of VM → cortex pathways (Kuramoto et al., 2015). Although species differences (rat vs mouse) may contribute to the results, technical differences may be a greater factor. In particular, our measurements were of electrophysiological connections, not anatomical projections, and involved sampling from a potentially large population of presynaptic terminals, not single axons. It is also important to consider that the ALM and M1 are located relatively far apart in the frontal cortex, at its rostral-most and caudal-most extents, respectively. The extent to which VM projections to motor areas located between ALM and M1 are anatomically and functionally segregated remains to be determined. Nevertheless, our findings indicate that the thalamic part of the recurrent loop involving ALM is restricted to an ALM-associated medial subdivision of VM, distinct from an M1-associated lateral subdivision of VM. Thus, the connectivity patterns reported here appear broadly consistent with the concept of parallel pathway organization proposed for premotor pathways based on studies in nonhuman primates (Strick, 1986; Middleton and Strick, 2000).

References

Acsády L (2017) The thalamic paradox. Nat Neurosci 20:901–902. CrossRef Medline

Alcaraz F, Marchand AR, Courtand G, Coutureau E, Wolff M (2016) Parallel inputs from the mediodorsal thalamus to the prefrontal cortex in the rat. Eur J Neurosci 44:1972–1986. CrossRef Medline

Alcaraz F, Fresno V, Marchand AR, Kremer EJ, Coutureau E, Wolff M (2018) Thalamocortical and corticothalamic pathways differentially contribute to goal-directed behaviors in the rat. eLife 7:e32517. CrossRef Medline

Apicella AJ, Wickersham IR, Seung HS, Shepherd GMG (2012) Laminarly orthogonal excitation of fast spiking and low threshold spiking interneurons in mouse motor cortex. J Neurosci 32:7021–7033. CrossRef Medline

Arbuthnott GW, MacLeod NK, Maxwell DJ, Wright AK (1990) Distribution and synaptic contacts of the cortical terminals arising from neurons in the rat ventromedial thalamic nucleus. Neuroscience 38:47–60. CrossRef Medline

Bortone DS, Olsen SR, Scanziani M (2014) Translaminar inhibitory cells recruited by layer 6 corticothalamic neurons suppress visual cortex. Neuron 82:474–485. CrossRef Medline

Bosch-Bouju C, Hyland BI, Parr-Brownlie LC (2013) Motor thalamus integration of cortical, cerebellar and basal ganglia information: implications for normal and parkinsonian conditions. Front Comput Neurosci 7:163. CrossRef Medline

Clascá F, Rubio-Garrido P, Jabaudon D (2012) Unveiling the diversity of thalamocortical neuron subtypes. Eur J Neurosci 35:1524–1532. CrossRef Medline

Collins DP, Anastasiades PG, Marlin JJ, Carter AG (2018) Reciprocal circuits linking the prefrontal cortex with dorsal and ventral thalamic nuclei. Neuron 98:366–379.e4. CrossRef Medline

Cruikshank SJ, Ahmed OJ, Stevens TR, Patrick SL, Gonzalez AN, Elmaleh M, Connors BW (2012) Thalamic control of layer 1 circuits in prefrontal cortex. J Neurosci 32:17813–17823. CrossRef Medline

Delevich K, Tucciarone J, Huang ZJ, Li B (2015) The mediodorsal thalamus drives feedforward inhibition in the anterior cingulate cortex via parvalbumin interneurons. J Neurosci 35:5743–5753. CrossRef Medline

Economo MN, Viswanathan S, Tasic B, Bas E, Winnubst J, Menon V, Graybuck LT, Nguyen TN, Wang L, Gerfen CR, Chandrashekar J, Zeng H, Looger LL, Svoboda K (2018) Distinct descending motor cortex pathways 1 and their roles in movement 2. bioRxiv. Advance online publication. Retrieved August 24, 2018. doi:10.1101/229260.

Gao Z, Davis C, Thomas AM, Economo MN, Abrego AM, Svoboda K, De Zeeuw CI, Li N (2018) A cortico-cerebellar loop for motor planning. Nature, in press.

Gerfen CR, Paletzki R, Heintz N (2013) GENSAT BAC cre-recombinase driver lines to study the functional organization of cerebral cortical and basal ganglia circuits. Neuron 80:1368–1383. CrossRef Medline

Goldman-Rakic PS (1995) Cellular basis of working memory. Neuron 14:477–485. CrossRef Medline

Gong S, Doughty M, Harbaugh CR, Cummins A, Hatten ME, Heintz N, Gerfen CR (2007) Targeting cre recombinase to specific neuron populations with bacterial artificial chromosome constructs. J Neurosci 27:9817–9823. CrossRef Medline

Grant E, Hoerder-Suabedissen A, Molnár Z (2016) The regulation of corticofugal fiber targeting by retinal inputs. Cereb Cortex 26:1336–1348. CrossRef Medline

Groenewegen HJ, Witter MP (2004) Thalamus. In: The rat nervous system (Paxinos G, ed), pp 407–453. Amsterdam, the Netherlands: Elsevier.

Guo ZV, Li N, Huber D, Ophir E, Gutnisky D, Ting JT, Feng G, Svoboda K (2014) Flow of cortical activity underlying a tactile decision in mice. Neuron 81:179–194. CrossRef Medline

Guo ZV, Inagaki HK, Daie K, Druckmann S, Gerfen CR, Svoboda K (2017) Maintenance of persistent activity in a frontal thalamocortical loop. Nature 545:181–186. CrossRef Medline

Harris KD, Shepherd GMG (2015) The neocortical circuit: themes and variations. Nat Neurosci 18:170–181. CrossRef Medline

Herkenham M (1979) The afferent and efferent connections of the ventromedial thalamic nucleus in the rat. J Comp Neurol 183:487–517. CrossRef Medline

Hooks BM, Mao T, Gutnisky DA, Yamawaki N, Svoboda K, Shepherd GMG

(2013) Organization of cortical and thalamic input to pyramidal neurons in mouse motor cortex. J Neurosci 33:748–760. CrossRef Medline

Inagaki HK, Inagaki M, Romani S, Svoboda K (2018) Low-dimensional and monotonic preparatory activity in mouse anterior lateral motor cortex. J Neurosci 38:4163–4185. CrossRef Medline

Jackman SL, Beneduce BM, Drew IR, Regehr WG (2014) Achieving high-frequency optical control of synaptic transmission. J Neurosci 34:7704–7714. CrossRef Medline

Jeong M, Kim Y, Kim J, Ferrante DD, Mitra PP, Osten P, Kim D (2016) Comparative three-dimensional connectome map of motor cortical projections in the mouse brain. Sci Rep 6:20072. CrossRef Medline

Jones EG (1975) Lamination and differential distribution of thalamic afferents within the sensory-motor cortex of the squirrel monkey. J Comp Neurol 160:167–203. CrossRef Medline

Jones EG (1998) Viewpoint: the core and matrix of thalamic organization. Neuroscience 85:331–345. CrossRef Medline

Jones EG (2001) The thalamic matrix and thalamocortical synchrony. Trends Neurosci 24:595–601. CrossRef Medline

Jones EG (2007) The thalamus, Ed 2. Cambridge: Cambridge UP.

Kase D, Uta D, Ishihara H, Imoto K (2015) Inhibitory synaptic transmission from the substantia nigra pars reticulata to the ventral medial thalamus in mice. Neurosci Res 97:26–35. CrossRef Medline

Kawaguchi Y (2017) Pyramidal cell subtypes and their synaptic connections in layer 5 of rat frontal cortex. Cereb Cortex 27:5755–5771. CrossRef Medline

Kita T, Kita H (2012) The subthalamic nucleus is one of multiple innervation sites for long-range corticofugal axons: a single-axon tracing study in the rat. J Neurosci 32:5990–5999. CrossRef Medline

Komiyama T, Sato TR, O'Connor DH, Zhang YX, Huber D, Hooks BM, Gabitto M, Svoboda K (2010) Learning-related fine-scale specificity imaged in motor cortex circuits of behaving mice. Nature 464:1182–1186. CrossRef Medline

Kuramoto E, Furuta T, Nakamura KC, Unzai T, Hioki H, Kaneko T (2009) Two types of thalamocortical projections from the motor thalamic nuclei of the rat: a single neuron-tracing study using viral vectors. Cereb Cortex 19:2065–2077. CrossRef Medline

Kuramoto E, Ohno S, Furuta T, Unzai T, Tanaka YR, Hioki H, Kaneko T (2015) Ventral medial nucleus neurons send thalamocortical afferents more widely and more preferentially to layer 1 than neurons of the ventral anterior-ventral lateral nuclear complex in the rat. Cereb Cortex 25:221–235. CrossRef Medline

Labarrera C, Deitcher Y, Dudai A, Weiner B, Kaduri Amichai A, Zylbermann N, London M (2018) Adrenergic modulation regulates the dendritic excitability of layer 5 pyramidal neurons in vivo. Cell Rep 23:1034–1044. CrossRef Medline

Larkum M (2013) A cellular mechanism for cortical associations: an organizing principle for the cerebral cortex. Trends Neurosci 36:141–151. CrossRef Medline

Li N, Daie K, Svoboda K, Druckmann S (2016) Robust neuronal dynamics in premotor cortex during motor planning. Nature 532:459–464. CrossRef Medline

Llinás R, Urbano FJ, Leznik E, Ramírez RR, van Marle HJ (2005) Rhythmic and dysrhythmic thalamocortical dynamics: GABA systems and the edge effect. Trends Neurosci 28:325–333. CrossRef Medline

Lörincz A, Notomi T, Tamás G, Shigemoto R, Nusser Z (2002) Polarized and compartment-dependent distribution of HCN1 in pyramidal cell dendrites. Nat Neurosci 5:1185–1193. CrossRef Medline

Luo L, Callaway EM, Svoboda K (2008) Genetic dissection of neural circuits. Neuron 57:634–660. CrossRef Medline

Madisen L, Garner AR, Shimaoka D, Chuong AS, Klapoetke NC, Li L, van der Bourg A, Niino Y, Egolf L, Monetti C, Gu H, Mills M, Cheng A, Tasic B, Nguyen TN, Sunkin SM, Benucci A, Nagy A, Miyawaki A, Helmchen F, et al (2015) Transgenic mice for intersectional targeting of neural sensors and effectors with high specificity and performance. Neuron 85:942–958. CrossRef Medline

Major G, Larkum ME, Schiller J (2013) Active properties of neocortical pyramidal neuron dendrites. Annu Rev Neurosci 36:1–24. CrossRef Medline

Middleton FA, Strick PL (2000) Basal ganglia output and cognition: evidence from anatomical, behavioral, and clinical studies. Brain Cogn 42:183–200. CrossRef Medline

Miesenböck G (2009) The optogenetic catechism. Science 326:395–399. CrossRef Medline

Mongillo G, Barak O, Tsodyks M (2008) Synaptic theory of working memory. Science 319:1543–1546. CrossRef Medline

Petreanu L, Mao T, Sternson SM, Svoboda K (2009) The subcellular organization of neocortical excitatory connections. Nature 457:1142–1145. CrossRef Medline

Qiu S, Anderson CT, Levitt P, Shepherd GMG (2011) Circuit-specific intracortical hyperconnectivity in mice with deletion of the autism-associated met receptor tyrosine kinase. J Neurosci 31:5855–5864. CrossRef Medline

Rojas-Piloni G, Guest JM, Egger R, Johnson AS, Sakmann B, Oberlaender M (2017) Relationships between structure, in vivo function and long-range axonal target of cortical pyramidal tract neurons. Nat Commun 8:870. CrossRef Medline

Rubio-Garrido P, Pérez-de-Manzo F, Clascá F (2007) Calcium-binding proteins as markers of layer-I projecting vs. deep layer-projecting thalamocortical neurons: a double-labeling analysis in the rat. Neuroscience 149:242–250. CrossRef Medline

Schoenenberger P, Schärer YP, Oertner TG (2011) Channelrhodopsin as a tool to investigate synaptic transmission and plasticity. Exp Physiol 96:34–39. CrossRef Medline

Sheets PL, Suter BA, Kiritani T, Chan CS, Surmeier DJ, Shepherd GMG (2011) Corticospinal-specific HCN expression in mouse motor cortex: ih-dependent synaptic integration as a candidate microcircuit mechanism involved in motor control. J Neurophysiol 106:2216–2231. CrossRef Medline

Shepherd GMG (2014) Diversity and complexity in the pyramidal tract projectome. Nat Rev Neurosci 15:63. CrossRef Medline

Strick PL (1975) Multiple sources of thalamic input to the primate motor cortex. Brain Res 88:372–377. CrossRef Medline

Strick PL (1986) The organization of thalamic inputs to the "premotor" areas. Prog Brain Res 64:99–109. CrossRef Medline

Strick PL, Sterling P (1974) Synaptic termination of afferents from the ventrolateral nucleus of the thalamus in the cat motor cortex. A light and electron microscopy study. J Comp Neurol 153:77–106. CrossRef Medline

Suter BA, Shepherd GMG (2015) Reciprocal interareal connections to corticospinal neurons in mouse M1 and S2. J Neurosci 35:2959–2974. CrossRef Medline

Suter BA, O'Connor T, Iyer V, Petreanu LT, Hooks BM, Kiritani T, Svoboda K, Shepherd GMG (2010) Ephus: multipurpose data acquisition software for neuroscience experiments. Front Neural Circuits 4:100. CrossRef Medline

Tervo DG, Hwang BY, Viswanathan S, Gaj T, Lavzin M, Ritola KD, Lindo S, Michael S, Kuleshova E, Ojala D, Huang CC, Gerfen CR, Schiller J, Dudman JT, Hantman AW, Looger LL, Schaffer DV, Karpova AY (2016) A designer AAV variant permits efficient retrograde access to projection neurons. Neuron 92:372–382. CrossRef Medline

Wang XJ (1999) Synaptic basis of cortical persistent activity: the importance of NMDA receptors to working memory. J Neurosci 19:9587–9603. CrossRef Medline

Wang XJ (2001) Synaptic reverberation underlying mnemonic persistent activity. Trends Neurosci 24:455–463. CrossRef Medline

Wang Y, Markram H, Goodman PH, Berger TK, Ma J, Goldman-Rakic PS (2006) Heterogeneity in the pyramidal network of the medial prefrontal cortex. Nat Neurosci 9:534–542. CrossRef Medline

Xu NL, Harnett MT, Williams SR, Huber D, O'Connor DH, Svoboda K, Magee JC (2012) Nonlinear dendritic integration of sensory and motor input during an active sensing task. Nature 492:247–251. CrossRef Medline

Yamawaki N, Shepherd GMG (2015) Synaptic circuit organization of motor corticothalamic neurons. J Neurosci 35:2293–2307. CrossRef Medline

Yamawaki N, Borges K, Suter BA, Harris KD, Shepherd GMG (2014) A genuine layer 4 in motor cortex with prototypical synaptic circuit connectivity. eLife 3:e05422. CrossRef Medline

Yamawaki N, Suter BA, Wickersham IR, Shepherd GMG (2016) Combining optogenetics and electrophysiology to analyze projection neuron circuits. Cold Spring Harb Protoc. Advance online publication. Retrieved August 24, 2018. doi:10.1101/pdb.prot090084.